

Research paper

Turn-off fluorene-based chemosensor switch to Fe³⁺: Spectroscopic study, merit parameters, theoretical calculations, and its application in Brazilian ethanol fuel

Fabiane dos Santos Carlos^a, Letícia Aparecida da Silva^a, Cristiano Zanlorenzi^b, Fábio Souza Nunes^{a,*}

^a Grupo de Espectroscopia e Reatividade de Compostos de Coordenação, Departamento de Química, Universidade Federal do Paraná, Cx. Postal 19081, 81531-980 Curitiba, PR, Brazil

^b Laboratório Polímeros Paulo Scarpa, Departamento de Química, Universidade Federal do Paraná, Cx. Postal 19081, 81531-980 Curitiba, PR, Brazil



ARTICLE INFO

Keywords:

Fluorescent chemosensor
Molecular switch
Fe³⁺
DFT

ABSTRACT

Development of a new chemosensor is challenging, because it has to deliver sensitiveness, selectiveness, reproducibility, robustness, and the least number of interfering analytes. In this sense coordination chemistry can offer an attractive approach to the problem. Diethyl 2-(9-fluorenyl) malonate (DEFM) was found to be an efficient fluorosensor for Fe³⁺ ions in ethanolic solutions, showing fluorescence quenching of 99% in the concentration range of 0.1–1.0 μmol L⁻¹, and most importantly, with no effect of interfering ions. Theoretical calculations supported photoelectron transfer (PET) mechanism to explain the fluorescence suppression observed. The method passed several analytical tests and showed the limit of detection and the limit of quantification at 15.56 and 51.85 nmol L⁻¹, respectively. The sensor passed a series of analytical tests and proved to be an attractive low-cost approach for Fe³⁺ quantification in ethanol fuel.

1. Introduction

Iron is an essential element. According to the World Health Organization, it is found in levels from 0.5 to 50 mg L⁻¹ at natural waters [1]. The minimum daily requirement for iron ranges from about 10 to 50 mg/day [1]. A healthy adult has 40 to 160 mg of iron in their blood, indexes above or below this are a warning sign. Despite this importance, excess or deficiency of iron in specific types of cells or organs can cause serious health problems, such as anemia, cirrhosis, diabetes, chronic fatigue, and osteoporosis.

Another interesting aspect about iron is related to the use of ethanol as a fuel in automobiles because it is considered an undesired inorganic contaminant [2]. From the point of view of the quality of fuel ethanol, metal ions are considered inorganic contaminants in any concentration, since metallic species can accelerate the corrosion of engines or promote the formation of gums and sediments. However, there are specifications on ions such as iron (5 mg / kg), copper (0.07 mg / kg), sodium (2 mg / kg), chloride (1 mg / kg) and sulfate (4 mg / kg) that can be observed in quality control resolutions for fuel ethanol from regulatory agencies such as ANP (Brazilian agency), which makes it mandatory to determine

the levels of these ions within their maximum allowed limits [3].

Iron can be inserted in this organic matrix through the steps involved in ethanol production or the storage phase [2–4]. Despite being found in low concentrations, the presence of metal ions can compromise the good performance of the engines, especially those powered by ethanol-gasoline mixture, due to the formation of gums (insoluble solids) by peroxidation processes of hydrocarbons present in gasoline; or oxidative processes of engine components, leading to possible exhaust gas emissions such as carbon monoxide, one of those responsible for the aggravation of the greenhouse effect [5]. The selective and sensitive identification of iron has been of interest to many researchers, and several detections and quantification methods have been developed, for example, voltammetric, fluorimetric, and ICP-OES measurements [6–10]. Fluorimetric protocols have played an important role in the detection of metal ions due to their simplicity and high sensitivity [11–16]. Fluorescent sensors for Fe³⁺ have been continuously devised [17–20] but, so far, easy-to-make chemosensors, with a low limit of detection and extensive work range are limited, and hence are still an analytic challenge.

Fluorene and its derivatives are rigid aromatic molecules that

* Corresponding author.

E-mail address: fsnunes@ufpr.br (F. Souza Nunes).

<https://doi.org/10.1016/j.ica.2021.120511>

Received 29 March 2021; Received in revised form 30 June 2021; Accepted 1 July 2021

Available online 6 July 2021

0020-1693/© 2021 Elsevier B.V. All rights reserved.

fluoresce in the ultra-violet region with high quantum yield and, owing to their numerous applications, have been the topic of studies for a long time [21–25]. However, fluorene-derivatives that act as selective fluorescent chemosensors for the detection of metal ions, including Fe^{3+} , together with statistical tests of the detection methods, are not often reported [26–31]. In this context, this work presents the investigation of a turn-off chemosensor based on a fluorescent fluorene derivative (diethyl 2-(9-fluorenyl)malonate, DEFM, see Scheme 1) for detection of Fe^{3+} . The structural simplicity and undemanding preparation of DEFM, together with the fact that this molecule has never been reported as a fluorescent sensor, are noteworthy.

Density functional theory (DFT and TD-DFT) calculations were carried out and afforded a plausible explanation for the sensing mechanism. Also, wide analytical parameters such as a calibration curve, limits of detection and quantification, as well as, repeatability, intermediate precision, robustness, and recovery testes confirmed the good applicability for this chemosensor for Fe^{3+} , compared to similar systems of chemosensors [32–40]. Moreover, works that employed wide analytical tests are rare in literature, making this work more applicable in real systems.

2. Experimental section

2.1. Chemicals and materials

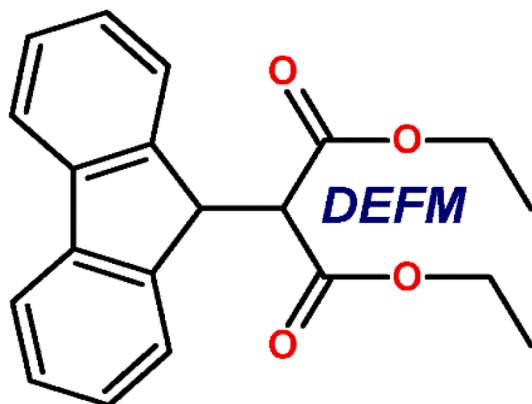
The chemicals are from Sigma-Aldrich and used as supplied. Before being used, all glassware was calibrated, washed by soaking in freshly prepared aqua regia ($1\text{HNO}_3/3\text{HCl}$ (v/v)) and then with ultrapure water, and finally dried in air.

2.2. Preparations

Diethyl 2-(9-fluorenyl) malonate (DEFM) was prepared as described elsewhere, Scheme 2 [41]. The yield was 62% (8.02 g). Elemental analysis found (calculated) for DEFM, $\text{C}_{20}\text{H}_{20}\text{O}_4$, 324.14 g mol^{-1} : C% 74.10 (74.06); H% 6.27 (6.21); N% 0.10 (0.00). ESI-MS (positive mode) at m/z – found (calculated): 325.14 (325.15) (molecular ion- H^+). The ^1H NMR, ^{13}C NMR, DEPT-135, and ESI-MS (including simulated) spectra are shown in the Supplementary Material, Figures SM1–SM3, with the appropriate assignments.

2.3. Apparatus

CHN analyses were carried out with a Perkin-Elmer 2400 analyzer. Mass spectra were measured in high-resolution ESI-MS on a microTOF QII mass spectrometer (Bruker Daltonics, Billerica) from solutions in ethanol. ^1H and ^{13}C NMR spectra were recorded on a Bruker Avance HD



Scheme 1. Representation of the chemosensor DEFM.

at 400 MHz, with CHCl_3 , and tetramethylsilane (TMS) as an internal reference. Chemical shifts are expressed in δ (ppm). Electronic spectra in the UV–Vis range (190–820 nm) were obtained on a diode array Hewlett Packard 8452A spectrophotometer in ethanol solutions using a 1.0 cm path length quartz cell.

Fluorescence measurements and fluorescence quantum yields were recorded at room temperature with a 1.0 cm optical path quartz cuvette using a Shimadzu RF5301-PC spectrofluorimeter. The equipment was set in between 1.5 and 5.0 nm slit width for excitation and emission spectra, employing a 600 nm min^{-1} scan rate and maximum wavelengths of excitation and emission at 296 nm and 316 nm, respectively.

DFT was carried out with the B3LYP functional and 6–311 g(d,p) basis to all atoms. The solvent was included (ethanol) in the calculation using SCRF formalism. Calculations were done using the Gaussian 09 [42]. Orbitals surfaces and population were obtained by Avogadro [43] and GaussSum 3.0 [44], respectively.

2.4. Sensitivity and selectivity measurements, and merit parameters

The selectivity was tested from a stock solution of DEFM (10 mmol L^{-1}) in ethanol, various dilutions were made to attain the working solution concentrations. The following species were used to evaluate the selectivity of the DEFM chemosensor: NH_4^+ , $[\text{N}(\text{CH}_3)_4]^+$, Li^+ , Na^+ , K^+ , Mg^{2+} , Ca^{2+} , Eu^{3+} , Tb^{3+} , Ru^{3+} , Co^{2+} , Ni^{2+} , Cu^{2+} , Zn^{2+} , Hg^{2+} , Cd^{2+} , Mn^{2+} , Fe^{3+} , Cr^{3+} and Al^{3+} they were accessed from the respective chloride salts in 10 mmol L^{-1} alcoholic stock solutions.

The sensitivity of DEFM for Fe^{3+} ions was determined from an analytical curve, which includes calculation of limit of detection (LOD) and quantification (LOQ). Merit parameters such as repeatability, intermediate precision, robustness, and recovery were calculated, using statistical approaches, to evaluate the analytical method, such as Grubbs, Fisher, Cochran, and Durbin-Watson tests [45–48]. Ethanol was employed as a solvent in all tests. Samples were measured in triplicate and standard variations were calculated from the results.

3. Results and discussion

3.1. Photophysics of the sensor DEFM

The photophysical and selectivity properties of sensor DEFM were carried out from alcoholic solutions. Absorption, excitation, and emission spectra are in Fig. 1. UV–vis spectra showed intraligand π - π^* and n - π^* transitions in the

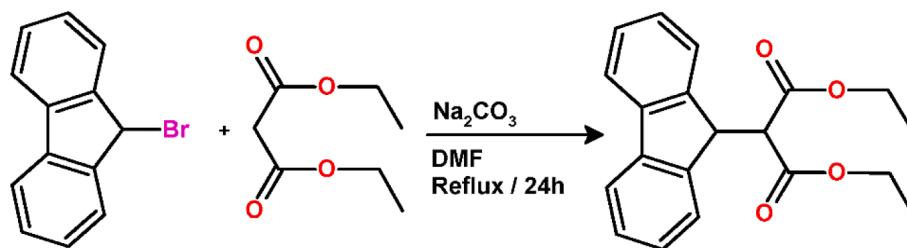
250–400 nm range, with maximum molar absorptivities of $1.21 \times 10^5\text{ L mol}^{-1}\text{ cm}^{-1}$ at 268 nm and of $8.65 \times 10^3\text{ L mol}^{-1}\text{ cm}^{-1}$ at 302 nm. When excited at 296 nm, which corresponds to the population of the first excited state $S_0 \rightarrow S_1$, the sensor emitted at 316 nm, with the highest efficiency.

3.2. Fluorimetric evaluation towards cations

3.2.1. Individual and collective selectivity

The majority of the tested cations did not change significantly the fluorescence of sensor DEFM, except for Fe^{3+} which caused a strong suppression of 99% as observed in Fig. 2(top), suggesting the formation of a complex formed in solution with high specificity for this metal ion and low values of the standard deviation. Individual selectivity was investigated upon quantitative addition of $100\text{ }\mu\text{mol L}^{-1}$ solutions of metal ions to equimolar solutions of the sensor DEFM.

In a collective selectivity test (Fig. 2 bottom), all cations used in the individual selectivity tests were tested together as potential interferences for the determination of Fe^{3+} . It shows the high specificity of the chemosensor towards Fe^{3+} ions since the set of cations did not interfere significantly with the suppression of the Fe^{3+} -DEFM complex. Furthermore, notice that Fe^{3+} produces a 99% quenching of fluorescence of the sensor, while it was reduced to 86% in presence of 21 metal



Scheme 2. (Top) Representation of the PET effect that quenches the fluorescence of the sensor DEFM upon coordination with Fe^{3+} , high spin, $2S+1 = 6$. (Bottom) Illustrative scheme of the PET redox process for the complex with 99% of quenching.

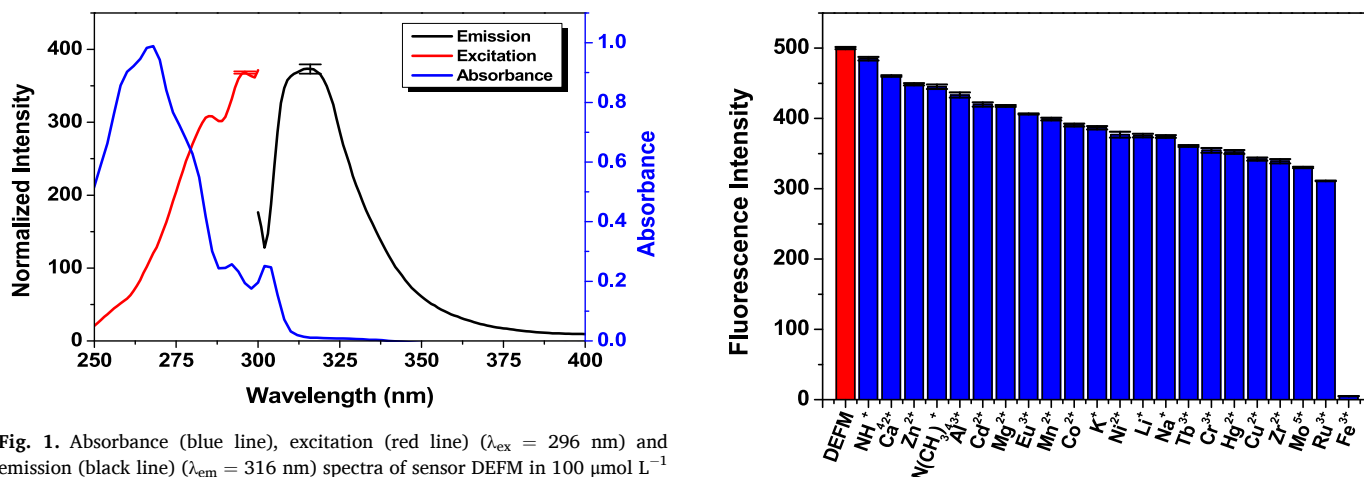


Fig. 1. Absorbance (blue line), excitation (red line) ($\lambda_{\text{ex}} = 296 \text{ nm}$) and emission (black line) ($\lambda_{\text{em}} = 316 \text{ nm}$) spectra of sensor DEFM in $100 \mu\text{mol L}^{-1}$ and ethanol. Excitation and emission slits are both 3 nm. (For interpretation of the references to colour in this figure legend, the reader is referred to the web version of this article.)

cations. This outcome reflects multiple, simultaneous equilibria of complex formation that are established in the presence of the different cations used. Under this condition, the concentration of $[\text{Fe}(\text{DEFM})_2\text{Cl}_2]^+$ in solution is reduced, which accounts for the increase of the fluorescence, compared to that observed in the competition tests (Fig. 2 top), carried out in the presence of individual ions. Testing the selectivity of DEFM in the presence of several different contaminants offers the best simulation of a potential application of the sensor in real samples, as opposed to the experiment in the presence of individual cations.

Finally, in the collective selectivity test, upon adding DEFM and 21 metal cations (except Fe^{3+}), the fluorescence intensity goes down by 57%. While the metal cation (other than Fe^{3+}) that lowers the fluorescence intensity the most is Ru^{3+} by $\sim 30\%$. The reason for that behavior is directly associated with the stability of the metal complexes formed in solution, which is given by their specific formation constants. In the presence of a mixture of metal ions, it is expected the formation of multiple equilibria. The particular stability of each complex influences the energy of the frontier orbitals, and consequently the ability to affect the PET mechanism. Thus, the suppression of the luminescence intensity is, indeed, expected to be different in the presence of a single metal ion of specific nature than in the presence of different cations.

3.2.2. Stoichiometry and stability of the Fe^{3+} -DEFM complex

The stoichiometry was determined by Job's plot for absorbance as seen in Fig. 3. The method showed a maximum absorption when the molar fraction of Fe^{3+} is close to 0.3, in accordance with the formation of a complex in a 1:2 (metal:sensor) ratio.

Benesi-Hildebrand [49], equation (1), allowed access to the binding constant for the complex, $1.5 \times 10^6 \text{ L}^2 \text{ mol}^{-2}$, for a 1:2 (metal:sensor)

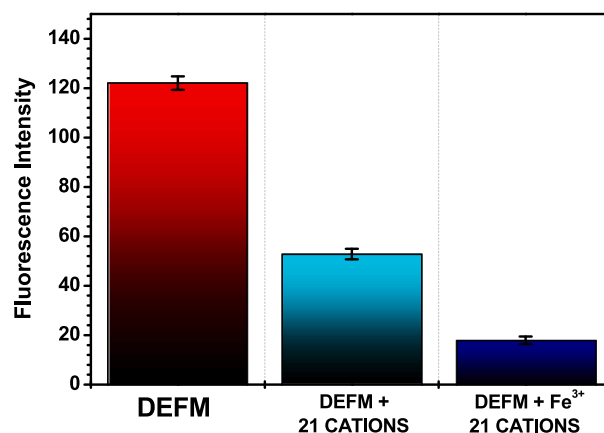


Fig. 2. (Top) Individual selectivity test: relative fluorescence of sensor DEFM in the presence of equimolar concentrations ($100 \mu\text{mol L}^{-1}$) of several cations in ethanolic solutions. Results are the average of triplicate measurements. Excitation (at 296 nm) and emission (at 316 nm) slits of 3 and 5 nm, respectively. (Bottom) Collective selectivity test, in the presence of equimolar concentrations ($100 \mu\text{mol L}^{-1}$) of all cations and sensor DEFM, in ethanol. Excitation and emission slits of 1.5 nm.

ratio as seen in Fig. 4(top). The high value of the formation constant supports a strong affinity of the sensor to the Fe^{3+} ion.

$$\frac{1}{F - F_0} = \frac{1}{(F_\infty - F_0)K[\text{Q}]^n} + \frac{1}{(F_\infty - F_0)} \quad (1)$$

where: F_0 and F = fluorescence of the sensor in the absence and presence of quencher; $[\text{Q}]$ = quencher concentration of Fe^{3+} ion; n = relation of Fe^{3+} ion and sensor ($=0.5$); K = binding constant of complex formed.

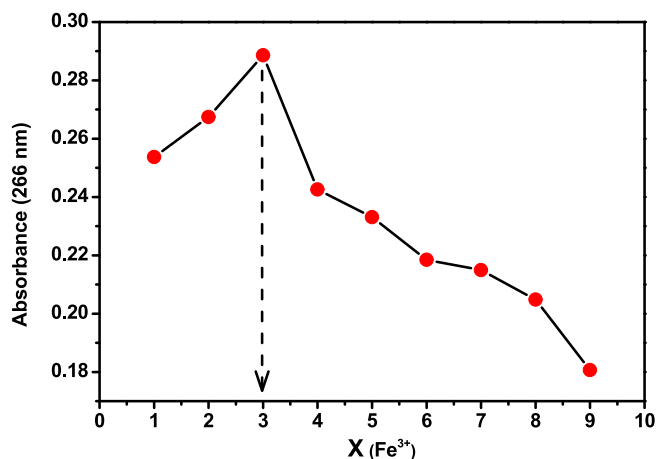


Fig. 3. Job's plot of the variation of the absorption at 266 nm for sensor DEFM and Fe³⁺ in a total molar concentration of 10 μmol L⁻¹ in ethanol.

Interaction of Fe³⁺ ion with the sensor DEFM was studied using Stern-Volmer's formalism [50] in accordance with a 1:2 (metal:sensor) stoichiometry given by the equation (2). A plot of $F-F_0$ versus [Fe³⁺] exhibited a linear fit with an R² of 0.9942, from 1.00 to 6.00 × 10⁻⁷ mol L⁻¹ of Fe³⁺ concentration. The linearity of the Stern-Volmer plot indicates a dynamic quenching mechanism, however the proximity between the values of K_{SV} and K at 1.0 × 10⁶ L² mol⁻² and 1.5 × 10⁶ L² mol⁻² respectively, also suggests some static suppression during the formation of the complex in the ground state.

$$\frac{F_0}{F} = 1 + k_q\tau_f[Q] = 1 + K_{SV}[Q]^n \quad (2)$$

where: F₀ and F = fluorescence of the sensor in the absence and presence of quencher, respectively; [Q] = quencher concentration of Fe³⁺; n = molar relation between Fe³⁺ ion and sensor (=0.5); k_q = bimolecular quenching constant, τ_f = lifetime of fluorescence in the absence of the quencher; K_{SV} = Stern-Volmer's suppression constant, which measures the metal:sensor affinity.

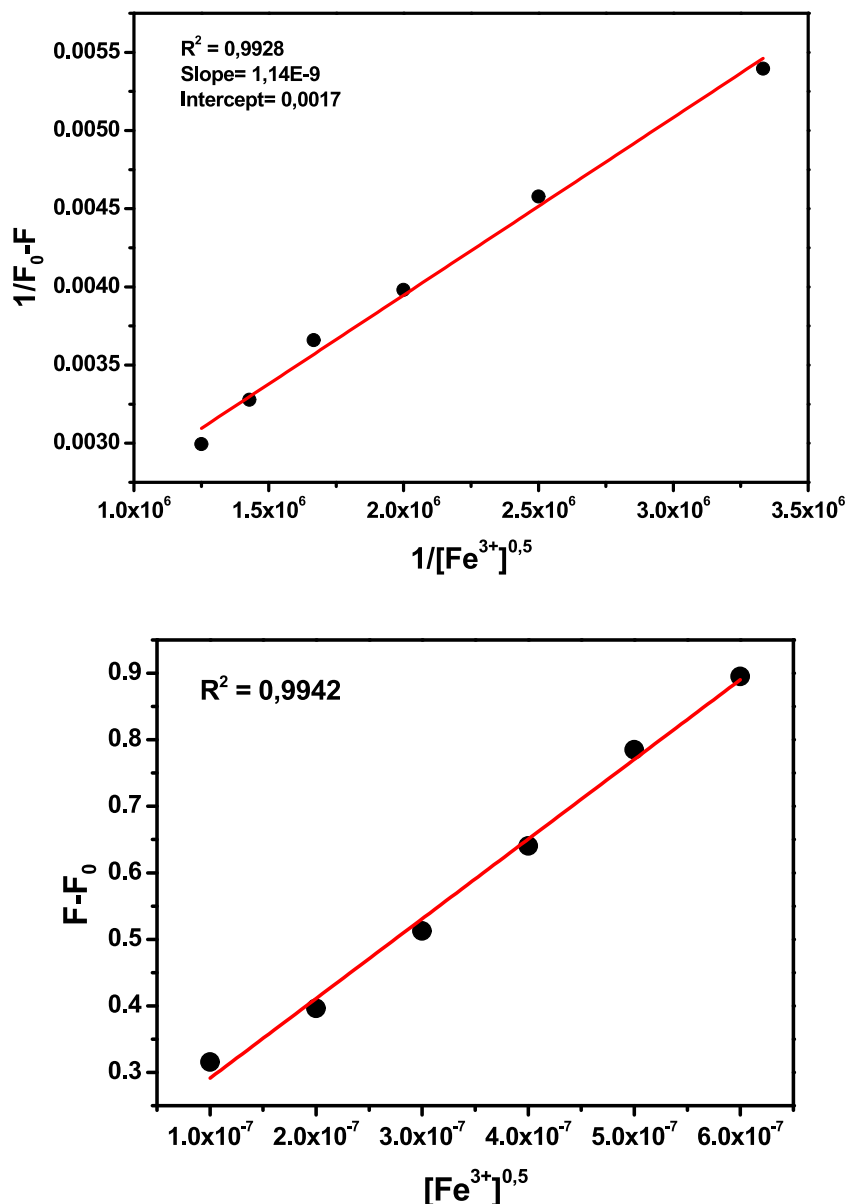


Fig. 4. (Top) Benesi-Hildebrand's plot for calculation of binding constant (K). (Bottom) Stern-Volmer's plot for calculation of suppression constant (K_{SV}).

3.2.3. Theoretical calculations

To better understand the electronic processes in molecular systems, such as emission and absorption processes, theoretical calculations are a valuable tool, that permits to access the energy diagram and their molecular orbitals involved in electronic transitions. The optimized geometries of the sensor and the Fe^{3+} complex, named $[\text{FeCl}_2(\text{DEFM})_2]^+$ with octahedral configuration, are shown in Fig. 5 (the coordinates of the optimized geometries are showed in Table SM1) along with the energy diagram in Fig. 6, and the most important electronic transitions are summarized in Table 1.

According to the ligand field applied by the ligands, the Fe^{3+} complex can present spin multiplicities of doublet and sextet (ground state), and quartet in excited states, depending on the different possibilities of matching the 5 electrons in the d orbitals. The theoretical calculations performed (under the unrestricted mode) investigated the absorption profile (Fig. SM4), from the first 150 transitions, simulating the three possibilities of spin state, and showed that the electronic energy of the sextet state is about 85.02 kJmol^{-1} less than the first quartet state, and 82.50 kJmol^{-1} more stable than the doublet state. This way, the following discussion about the observed suppression phenomena will be referred to the sextet state.

Also, it was investigated the stability of complex $[\text{FeCl}_2(\text{DEFM})_2]^+$ based on the free energy calculations obtained from optimized geometries of reactants and products, and the results revealed a free energy of $-1239 \text{ kJ mol}^{-1}$ for $[\text{FeCl}_2(\text{DEFM})_2]^+$.

It should be pointed out the good correspondence between the calculated and the experimental absorption spectra (Table 1) of the free sensor (Fig. 1) and its complex (Fig. SM4) that show mainly intraligand transitions. An inspection of the molecular orbital diagram of DEFM in Fig. 6 shows that

HOMO(-6.23 eV) and LUMO + 3(-0.21 eV) are mainly centered on the fluorene unit, thus the excitation at 296 nm, through a $\pi-\pi^*$ transition is followed by the reverse process, which accounts for the fluorescence of the free sensor. In contrast, excitation of the complex $[\text{FeCl}_2(\text{DEFM})_2]^+$ at 296 nm is associated with the transition HOMO-12(-9.05 eV) \rightarrow LUMO + 3(-1.59 eV) (the first has major contributions are from malonate and the chloride ions, while the second is centered in the malonate unit). Therefore, after the photo-excitation of the complex at 296 nm, an electron from HOMO(-6.93 eV) can be transferred to HOMO-12(-9.05 eV), through the photoinduced electron transfer (PET) mechanism [51,52] (See Scheme 3), drastically decreasing the fluorescence intensity observed, also known as an ON-OFF fluorescent switch [53-57]. The complete set of orbitals for both DEFM and its Fe^{3+} can be found in the Supplementary Material Section, Table SM2)

Thus, coordination of the sensor with Fe^{3+} inhibits the back electron transfer observed in the free ligand from LUMO + 3 to HOMO orbitals, thus turning off the fluorescence [53]. Besides this static quenching, Fe^{3+} can provoke a nonradiative deactivation of the sensor, as suggested by the Stern-Volmer analysis (Fig. 4), and has been proposed as an

alternative mechanism for the quenching of fluorophores [54]. Interestingly to note that for a ground state with $2S + 1 = 2$ (Fe^{3+} , low spin), the excitation of at the same wavelength (296 nm) excites an electron from the HOMO-12(-8.57 eV)(centered in the chloride ligand) to the LUMO(-3.57 eV)(which has significant contribution of the dz^2 of Fe^{3+} , Fig. SM5). In that case, thus, the static quenching is associated with a LMCT transition.

3.3. Evaluation of the analytical method

3.3.1. Calibration curve and the sensibility of sensor

Limit of detection (LOD) (3 s/l, where: s = standard deviation; I = slope of the line) and limit of quantification (LOQ = 10 s/l) were calculated from the analytical curve shown in Fig. 7. LOD and LOQ were found at 15.56 and $51.85 \text{ nmol L}^{-1}$, respectively, within linearity of $0.1-1.0 \text{ } \mu\text{mol L}^{-1}$ ($R^2 = 0.997$, least squares method). The quality of the correlation between the concentration of the Fe^{3+} ion and the intensity of emission were checked by several statistical tests (Grubb's, Fisher's, Cochran's, Durbin-Watson's test) described in the Supplementary section of the manuscript (Tables SM3-SM6, equations SM1-SM4). The tests were approved and recommended by regulatory agencies [45-48,58].

3.3.2. Repeatability and intermediate precision tests

Results of the repeatability and intermediate precision tests [45-48,58] are summarized in Table SM7 for the lower level of concentration for detection of Fe^{3+} ions with precision and accuracy, therefore using the limit of quantification ($\sim 51.85 \text{ nmol L}^{-1}$), using ten replicate measurements, Fig. 8(left). The intermediate precision tests out the accordance of the results from the same laboratory (repeatability and analyst 1) but performed by a different analyst (analyst 2). All the samples showed a HorRat ratio ($RSD/RSD_{Horwitz}$) lower than 1, and thus approved in the test. The Fisher's test also gives that $F_{calc}(\text{analyst 1}; \text{analyst 2}) = 0.52$, which is lower than $F_{critical} = 4.03$, hence supporting that the analytical method is reproducible and repeatable.

3.3.3. Robustness of sensor DEFM

The robustness was evaluated by Youden's test [45-48,58] from fractional factorial planning using 8 different combinations of seven nominal experimental conditions, duplicate measurements (see Tables SM8-SM10). So each condition was varied 4 times in four different combinations, and with that, it was possible to calculate the error of the measurements in the various conditions (equation (3)). These results are gathered within Pareto's graph in Fig. 8(right); as well as the calculation of the significance line, which corresponds to the maximum deviation allowed (equation (4)).

The chart shows the quality deviation for each condition within Youden's test, and showed no relevant significance, since they are below the maximum deviation calculated at 0.400 thus indicating the high robustness of the method.

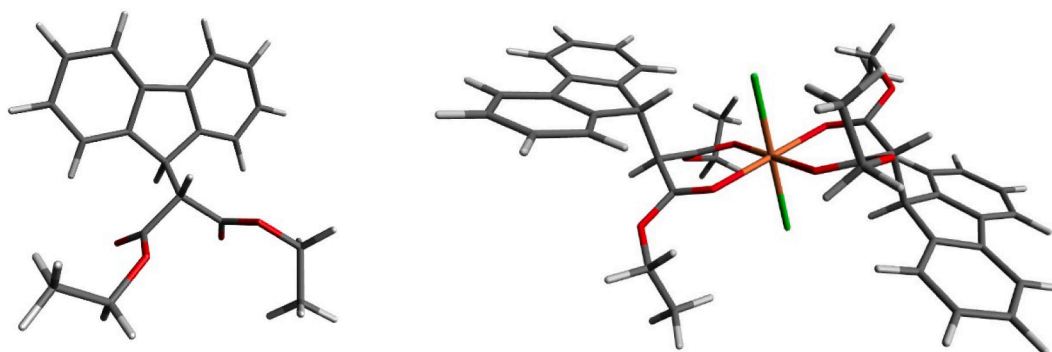


Fig. 5. Optimized geometries for DEFM chemosensor and their complex formed in solution, $[\text{FeCl}_2(\text{DEFM})_2]^+$.

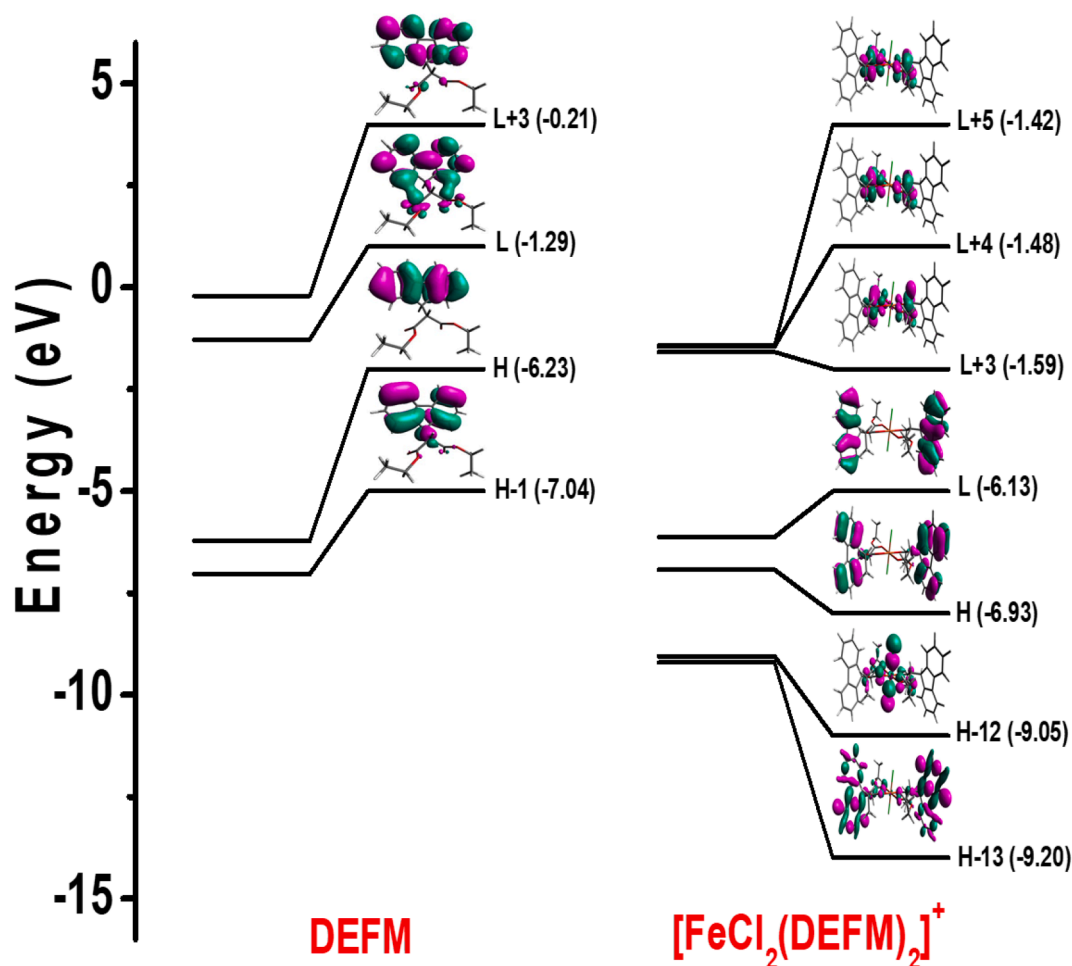


Fig. 6. Frontier molecular orbitals of the chemosensor DEFM and $[\text{FeCl}_2(\text{DEFM})_2]^+$.

Table 1
TD-DFT electronic transitions in DEFM and $[\text{FeCl}_2(\text{DEFM})_2]^+$.

Compound	Wavelength / nm (experimental)	Osc. Strength	Major contribution
DEFM	272 (302)	0.42	HOMO → LUMO
	217 (290)	0.21	HOMO → LUMO + 3
	193 (266)	0.75	HOMO-1 → LUMO + 3
$[\text{FeCl}_2(\text{DEFM})_2]^+$	347 (320)	0.09	HOMO-13 → LUMO
	286 (290)	0.10	HOMO-12 → LUMO + 3
	261 (302)	0.27	HOMO-13 → LUMO + 4
	267 (266)	0.66	HOMO → LUMO + 5

Considering that out of the 8 combinations performed for each investigated parameter, four were made with the nominal condition and four with the varied condition, then it was possible to apply the Fisher's test which compares the variances of both sets of data (equation SM2). For all nominal condition the result the value of F_{calc} (Table SM11) was less than $F_{\text{critical}} = 15.44$, considering a 95% of confidence level, hence supporting that the analytical method is robust.

$$\text{Effect of the temperature} = \frac{A + B + C + D}{4} - \frac{E + F + G + H}{4} \quad (3)$$

$$\text{Significance line} = t_{\text{critical}} * \sqrt{\frac{4 * s_n^2}{N}} \quad (4)$$

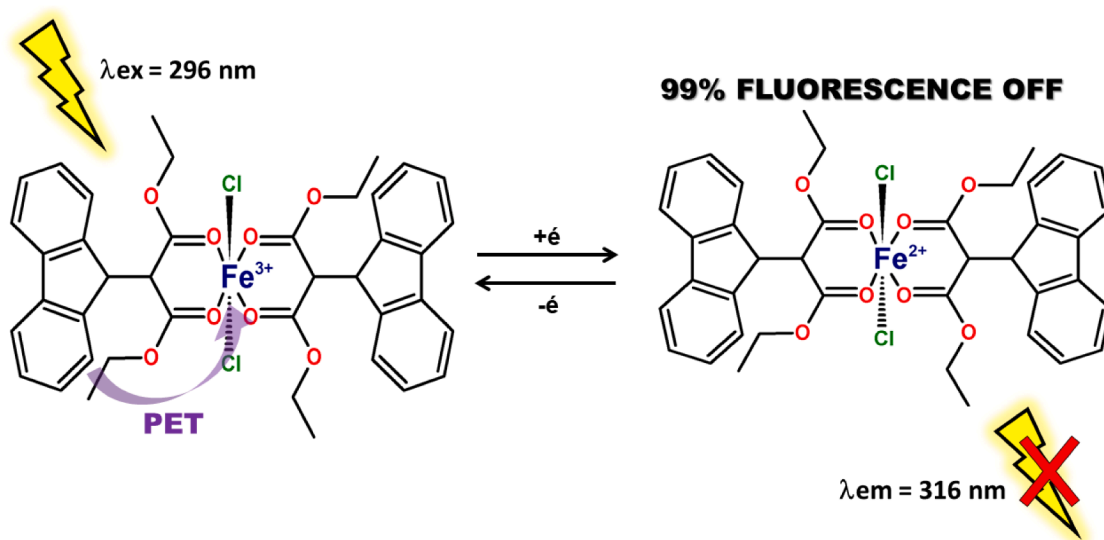
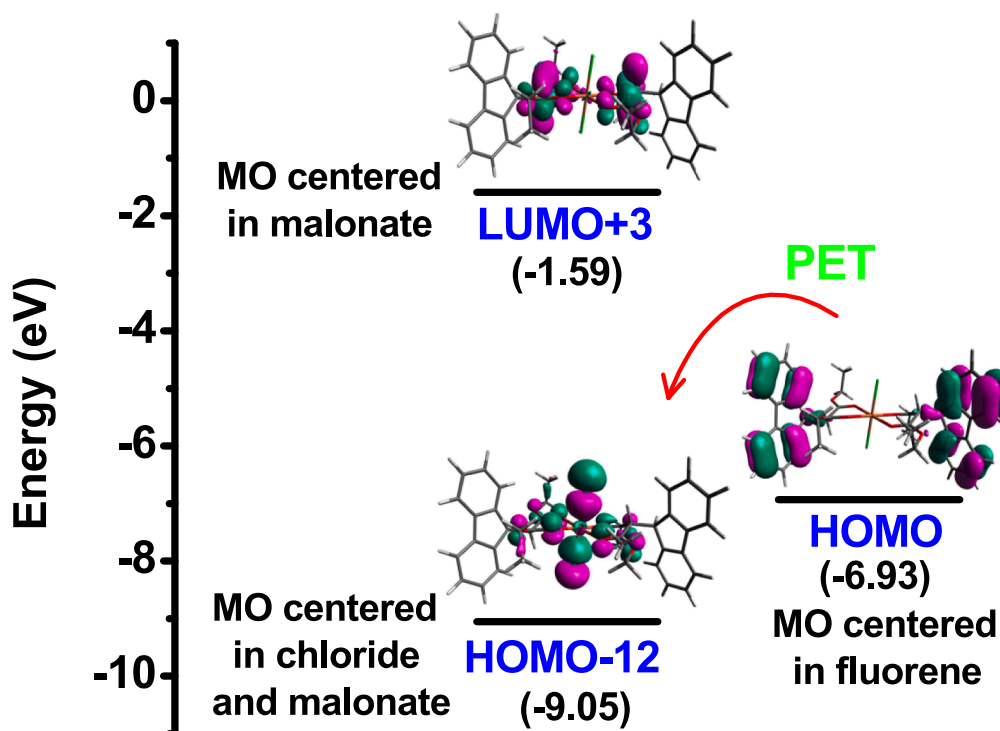
where: $t_{\text{critical}} = t$ student (2.36); s = standard deviation; $N = 16$.

3.3.4. Reversibility test

To study the reversibility of the sensor DEFM towards Fe^{3+} ions in ethanolic solutions, the fluorescence intensity of DEFM after successive addition of Fe^{3+} ions and EDTA was measured out (Fig. 9). The addition of one equivalent of Fe^{3+} to a solution of DEFM, resulted in a significant decrease of fluorescence intensity, because of the established equilibrium in favor of the formation of the $[\text{FeCl}_2(\text{DEFM})_2]^+$ complex. After the addition of one equivalent of EDTA to the system, the fluorescence of the solution increases due to the binding of EDTA to the free Fe^{3+} , while DEFM was released to the solution. The alternate addition of Fe^{3+} and EDTA to DEFM solution produced an on/off fluorescence response for at least two cycles, illustrating thus, the satisfactory reversibility of sensor DEFM with Fe^{3+} ions.

3.3.5. Practical application

The best performance of the DEFM sensor was observed when it is dissolved in ethanol. Therefore, recovery tests were carried out using ethanol fuel for automobiles from a gas station as a matrix, since it is known that it is contaminated with undesired Fe^{3+} ions. The samples were prepared as follows: To a 5.0 mL volumetric flask were added 50 μL of the stock solution of the sensor DEFM in ethanol (10 mmol L^{-1}) and 50 μL of a 500 $\mu\text{mol L}^{-1}$ stock solution of ferric chloride in ethanol ($10 \mu\text{mol L}^{-1}$). The final volume was completed to 5.0 mL with the matrix,



Scheme 3. Chemical equation for the preparation of DEFM.

and all measurements were triplicated. Results are gathered in Table 2, where satisfactory recovery values were observed in the range of 46–547% [45–48,58].

3.4. Comparison with similar sensors

Table 3 shows analytical data from some recently published sensors for Fe^{3+} . In all samples, the sensors are active in organic/inorganic media or a mixture of solvents. Among those examples, DEFM has the lowest limit of detection, low relative error, and the highest metal-to-

sensor binding constant. Moreover, it does not suffer interference from other ions and exhibits one of the best linear ranges. Also, it is the only study that presents merit parameters, such as repeatability, intermediate precision, robustness, and recovery that allows a thorough evaluation of the analytical usage of the DEFM sensor towards metal ions sensing.

4. Conclusions

A new sensor for selective and specific detection of Fe^{3+} was tested out for measurements in ethanolic solutions. Complex formation with

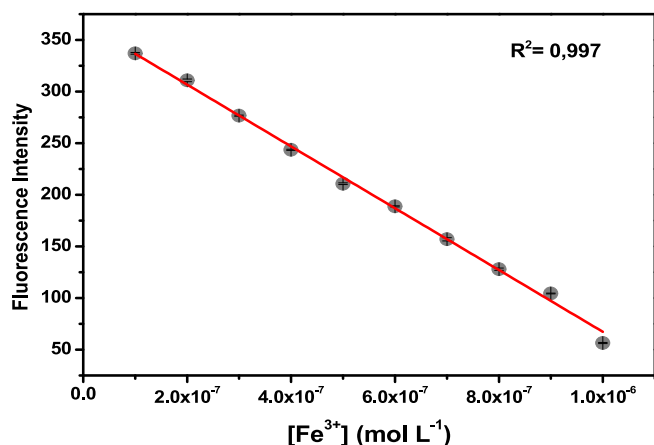


Fig. 7. Analytical curve for sensor DEFM. Results are the average of triplicate measurements. Excitation and emission slits are 3 and 5 nm, respectively.

Fe^{3+} led to a strong fluorescent quenching (99%), good linearity, and limit of detection of

$15.56 \text{ nmol L}^{-1}$. Job's and Benesi-Hildebrand's method relationships suggested a 1:2(metal:sensor) stoichiometry, with a fairly high association constant ($K = 1.5 \times 10^6 \text{ L}^2 \text{ mol}^{-2}$) reported for similar systems, thus proving the strong sensor:analyte affinity. Besides, Stern-Volmer's constant ($K_{SV} = 1.0 \times 10^6 \text{ L}^2 \text{ mol}^{-2}$) suggests a dynamic quenching, though the proximity of K and K_{SV} suggests some static suppression due to the complex formed in solution. Theoretical calculations suggested that the photoelectron transfer (PET) mechanism can explain the fluorescent suppression observed, a process which is associated with an intraligand charge transfer (ICT) and a LMCT, respectively, for the sextet, and doublet ground states of the Fe^{3+} complex. The fluorimetric method for detection and quantification of Fe^{3+} was further studied to check its quality and analytical applicability. The excellence of the analytical curve was confirmed through the application of a series of statistical tests. Furthermore, the practicability of the method passed the repeatability as well as intermediate precision, robustness, and recovery tests from fuel ethanol as a matrix. Finally, the sensor showed no common interfering ions, thus showed that the sensor DEFM can be successfully used to determine Fe^{3+} ions.

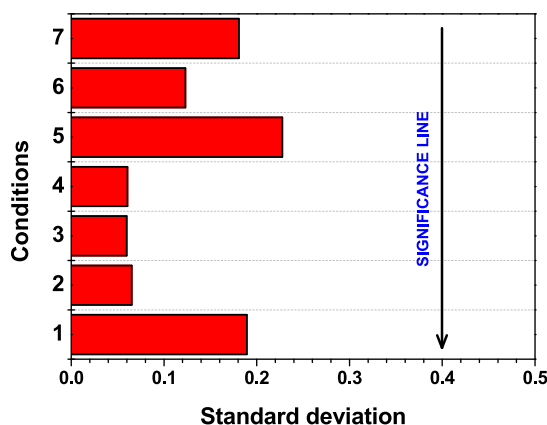
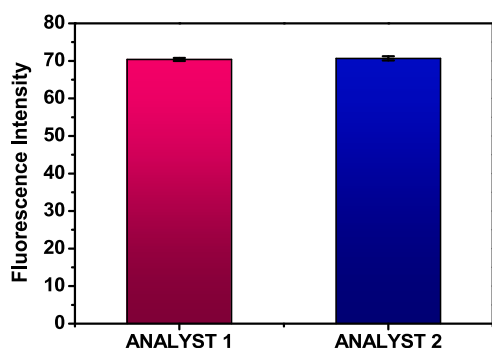


Fig. 8. (left) Repeatability and intermediate precision tests of Fe^{3+} ions. Colors refer to two different analysts and error bars apply to ten replicates. Slit is 3 nm. $[\text{Fe}^{3+}] = \text{LOQ}$, $[\text{DEFM}] = 10 \mu\text{mol L}^{-1}$; ethanol medium. (right) Pareto's graph, showing the changes in the measurement of experimental conditions for chemosensor DEFM. Conditions are: 1) temperature during measurement (room temperature and 10°C), 2) reagent supplier (SIGMA and MERCK), 3) time between sample preparation and measurement (2 and 1.5 h), 4) solvent supplier (DINAMICA and BIOTEC), 5) sample storage before measurements (room temperature and 15°C), 6) purge of the sample with inert gas (yes and no), 7) cleaning the cuvette between replicates (2xethanol + 1xacetone; versus only 1xacetone). The concentration of DEFM and Fe^{3+} ions were constant at 1.00×10^{-4} and $1.00 \times 10^{-6} \text{ mol L}^{-1}$, respectively.

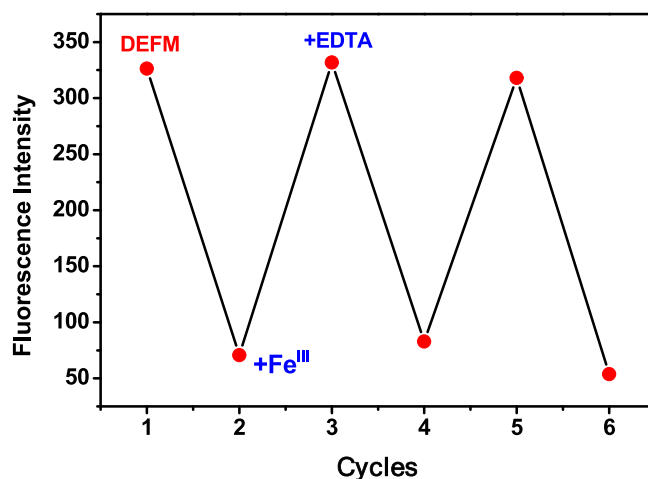


Fig. 9. Reversible fluorescence changes of sensor DEFM ($100 \mu\text{M}$; emission in 316 nm) in ethanol solution after successive addition of Fe^{3+} ($0.5 \mu\text{M}$) and EDTA ($0.5 \mu\text{M}$). Excitation and emission slits are both 1.5 nm .

Table 2

Recovery values (%) from solutions of DEFM and Fe^{3+} in ethanol fuel.

MATRIX	$[\text{Fe}^{3+}]$ (nmol L^{-1})	RECOVERY (%)
ETHANOL FUEL	100	45.99 ± 0.15
	500	96.60 ± 0.32
	1000	547.23 ± 0.88

CRediT authorship contribution statement

Fabiane Santos Carlos: Methodology, Investigation, Formal analysis, Visualization, Supervision. **Leticia Aparecida Silva:** Investigation, Validation. **Cristiano Zanlorenzi:** Software, Investigation, Visualization. **Fábio Souza Nunes:** Conceptualization, Resources, Writing - review & editing, Funding acquisition.

Declaration of Competing Interest

The authors declare that they have no known competing financial interests or personal relationships that could have appeared to influence

Table 3

Comparison between some fluorescent sensors for Fe³⁺. LOD = limit of detection. MP = merit parameters.

Sensor	LOD	Linear Range (μmol L ⁻¹)	Interfering Ions	Medium	logK	MP
DEFM	15.56 nmol L ⁻¹	0.1–1.0	none	ethanol	6.0	Yes
[28]	2.22 μmol L ⁻¹	200–1000	none	H ₂ O/tris-HCl	–	No
[34]	–	–	none	H ₂ O /DMF (5:5 v/v)	–	No
[32]	–	–	Cu ²⁺	THF	–	No
[35]	0.29 μmol L ⁻¹	20–100	Al ³⁺ , Ca ³⁺	H ₂ O/MeOH(1:1 v/v)	4.8	No
[19]	275 nmol L ⁻¹	0.1–50	none	H ₂ O	–	No
[18]	0.5 μmol L ⁻¹	40–160	Ni ²⁺ , Co ²⁺ , Mn ²⁺	DMF	–	No

the work reported in this paper.

Acknowledgements

Brazilian Research Council CNPq supported this work. F.S.N. and F.S.C. thank CNPq and CAPES for research fellowships. We gratefully thank Professor Leni Campos Akcelrud for allowing access to the spectrofluorimeter at Paulo Scarpa Laboratory, UFPR.

Appendix A. Supplementary data

Supplementary data to this article can be found online at <https://doi.org/10.1016/j.ica.2021.120511>.

References

- [1] World Health Organization (WHO). Guidelines for Drinking-water Quality incorporating the 1st and 2nd addenda, 3rd ed.; WHO: Geneva, 2008.
- [2] R.M. Takeuchi, A.L. Santos, N.R. Stradioto, P.M. Padilha, Copper determination in ethanol fuel by differential pulse anodic stripping voltammetry at a solid paraffin-based carbon paste electrode modified with 2-aminothiazole organofunctionalized silica, *Talanta* 71 (2007) 771–777.
- [3] Agência Nacional Do Petróleo (ANP). Especificações do etanol anidro combustível (EAC) e do etanol hidratado combustível (EHC); Brasil, 2015.
- [4] A.L. Santos, R.M. Takeuchi, N.R. Stradioto, L. Angnes, R.A.A. Muñoz, Electrochemical Determination of Inorganic Contaminants in Automotive Fuels, *Electroanalysis* 24 (2012) 1681–1691.
- [5] R.C.C. Pereira, V.M.D. Pasa, Effect of Alcohol and Copper Content on the Stability of Automotive Gasoline, *Energy Fuels* 19 (2005) 426–432.
- [6] J. Hou, Z. Sun, Z. Yang, L. Zhao, Y. Zhang, Y. Li, L. Ding, Microwave-assisted fabrication of multicolor photoluminescent carbon dots as a ratiometric fluorescence sensor for iron ions, *New J. Chem.* 43 (2019) 853–861.
- [7] M. Ak, R. Ayranci, An Electrochemical Sensor Platform for Sensitive Detection of Iron (III) Ions Based on Pyrene-Substituted Poly(2,5-dithienylpyrrole), *J. Electrochem. Soc.* 166 (2019) B291–B296.
- [8] A.L. Saber, A.M. Hameed, A.A. Saygal, H. Alessa, A. Alharbi, Iron-selective Poly (Vinyl Chloride) Membrane Electrode Based on Norfloxacin as a Neutral Carrier, *Int. J. Electrochem. Sci.* 13 (2018) 10076–10087.
- [9] Z.-A. Zonga, C.-B. Fana, C.-F. Bia, X. Zhang, R. Luoa, X.-M. Mengc, F. Jing, Y.-H. Fana, Highly selective functional luminescent sensor toward Cr(VI)/Fe(III) ion and nitrobenzene based on metal-organic frameworks: Synthesis, structures, and properties, *J. Solid State Chem.* 270 (2019) 651–665.
- [10] A.-Z. Hossein, Z.-K. Monireh, A turn-on/off fluorescent sensor based on nano-structured Mg-Al layered double hydroxide intercalated with salicylic acid for monitoring of ferric ion in human serum samples, *Anal. Chim. Acta* 1061 (2019) 152–160.
- [11] F.S. Carlos, M.C. Nunes, L.D. Boni, G.S. Machado, F.S. Nunes, A novel fluorene-derivative Schiff-base fluorescent sensor for copper(II) in organic media, *J. Photochem. Photobiol. A* 348 (2017) 41–46.
- [12] F.S. Carlos, C. Zanlorenzi, R.F. Monteiro, L.A. Silva, F.S. Nunes, A highly selective acridine-based fluorescent probe for detection of Al(III) in alcoholic beverage samples, *Spectrochim. Acta A* 231 (2020) 118–124.
- [13] M.C. Nunes, F.S. Carlos, O. Fuganti, F.S. Nunes, A Facile Preparation of a New Water-Soluble Acridine Derivative and Application as a Turn-off Fluorescence Chemosensor for Selective Detection of Hg₂⁺, *J. Fluoresc.* 30 (2020) 235–247.
- [14] M.C. Nunes, F.S. Carlos, O. Fuganti, D.D.M. Galindo, L.D. Boni, G. Abate, F. S. Nunes, Turn-off fluorescence study of a highly selective acridine-based chemosensor for Zn²⁺ in aqueous solutions, *Inorg. Chim. Acta* 499 (2020) 119191–119200.
- [15] F.S. Carlos, C. Zanlorenzi, L.A. Silva, F.S. Nunes, A novel macrocycle acridine-based fluorescent chemosensor for selective detection of Cd²⁺ in Brazilian sugarcane spirit and tobacco cigarette smoke extract, *Inorg. Chim. Acta* 508 (2020) 119634–119641.
- [16] F.S. Carlos, M.C. Nunes, B.A. Iglesias, P.J. Zambiasi, M. Hörner, G.A. Moraes, G. S. Machado, R.R. Ribeiro, F.S. Nunes, Fluorenyl-Schiff-base ligands and their dicopper(II) complexes. Synthesis, structural and spectroscopic characterization and DNA binding assays, *Polyhedron* 144 (2018) 18–29.
- [17] W.E. Jones, L.-J. Fan, A Highly Selective and Sensitive Inorganic/Organic Hybrid Polymer Fluorescence “Turn-on” Chemosensory System for Iron Cations, *J. Am. Chem. Soc.* 128 (2006) 6784–6785.
- [18] V. Safarifar, Y.D. Farahani, Highly selective detection of Fe³⁺, Cd²⁺ and CH₂Cl₂ based on a fluorescent Zn-MOF with azine-decorated pores, *J. Solid State Chem.* 275 (2019) 131–140.
- [19] Z. Mu, J. Hua, S. Feng, Y. Yang, A ratiometric fluorescence and light scattering sensing platform based on Cu-doped carbon dots for tryptophan and Fe(III), *Spectrochim. Acta A* 219 (2019) 248–256.
- [20] S. Ghosh, R. Manna, S. Dey, Epoxy-based polymer incorporating 1-naphthylamine and sebacic acid moieties: A selective fluorescent sensor for ferric ions, *J. Mol. Struct.* 1180 (2019) 406–410.
- [21] Rodrigues, P. C.; Fontes, B. D.; Torres, B. B. M.; Sousa, W. S.; Faria, G. C.; Balogh, D. T.; Faria, R. M.; Akcelrud, L. Synthesis of a PPV-fluorene derivative: Applications in luminescent devices. *J. Appl. Polym. Sci.* 2015, 42579–42586.
- [22] X. Cao, A. Gao, N. Zhao, F. Yuan, C. Liu, R. Li, Surfaces wettability and morphology modulation in a fluorene derivative self-assembly system, *Appl. Surf. Sci.* 368 (2016) 97–103.
- [23] K. Shanmugasundaram, M.S. Subeesh, C.D. Sunesh, R.K. Chitumalla, J. Jang, Y. Choe, Synthesis and photophysical characterization of an ionic fluorene derivative for blue light-emitting electrochemical cells, *Org. Electron.* 24 (2015) 297–302.
- [24] K. Baumgärtner, F. Rominger, M. Mastalerz, An Oxidative Macrocyclic Ring Opening of a Triptycene to a Highly Functionalized Fluorene Derivative, *J. Org. Chem.* 80 (2015) 8881–8886.
- [25] S.A. Kurhuzenkau, A.W. Woodward, S. Yao, K.D. Belfield, Y.O. Shaydyuk, C. Sissa, M.V. Bondar, A. Painelli, Ultrafast spectroscopy, superluminescence and theoretical modeling for a two-photon absorbing fluorene derivative, *Phys. Chem. Chem. Phys.* 18 (2016) 1239–1246.
- [26] J.L. Pablos, S. Ibeas, A. Muñoz, F. Serna, F.C. García, J.M. García, Solid polymer and metallogel networks based on a fluorene derivative as fluorescent and colourimetric chemosensors for Hg(II), *React. Funct. Polym.* 79 (2014) 14–23.
- [27] Q. Li, Y. Jia, Z. Feng, Liu, F., A highly sensitive and selective fluorescent probe without quencher for detection of Pb²⁺ ions based on aggregation-caused quenching phenomenon, *RSC Adv.* 8 (2018) 38929–38934.
- [28] L. Qi, Q. Chen, Z. Niu, X. Zhou, T. Yanga, W. Huang, Lanthanide metal-organic frameworks assembled from a fluorene-based ligand: selective sensing of Pb²⁺ and Fe³⁺ ions, *J. Mater. Chem. C* 4 (2016) 1900–1905.
- [29] A. Hens, K.K. Rajak, Selective fluorometric detection of F-1 and Zn(II) ions by a N, O coordinating sensor and naked eye detection of Cu(II) ions in mixed-aqueous solution, *RSC Adv.* 5 (2015) 44764–44777.
- [30] K. Belfield, M.V. Bondar, A. Frazer, A.R. Morales, O.D. Kachkovsky, I.A. Mikhailov, A.E. Masunov, O.V. Przhonska, Fluorene-Based Metal-Ion Sensing Probe with High Sensitivity to Zn²⁺ and Efficient Two-Photon Absorption, *J. Phys. Chem. A* 114 (2010) 9313–9321.
- [31] J. Cao, Y. Li, J. Feng, 9-Benzylidene-9H-fluorene Derivatives Linked to Monoaza-15-crown-5: Synthesis and Metal Ion Sensing, *Chin. J. Chem. Phys.* 30 (2012) 1571–1574.
- [32] P. Li, Y. Zhao, L. Yao, H. Nie, M. Zhang, A simple, selective, fluorescent iron(III) sensing material based on peripheral carbazole, *Sensor Actuat. B-Chem.* 191 (2014) 332–336.
- [33] C.-S. Wu, Y.-J. Lin, Y. Chen, A fluorene-based material containing triple azacrown ether groups: synthesis, characterization and application in chemosensors and electroluminescent devices, *Org. Biomol. Chem.* 12 (2014) 1419–1429.
- [34] C. Yi, B. Song, W. Tian, X. Cui, Q. Qi, W. Jiang, Z. Qi, Y. Sun, Fluorescent sensor of fluorene derivatives having phosphonic acid as a fluorogenic ionophore: synthesis and static quenched properties for Fe(III), *Tetrahedron Lett.* 55 (2014) 5119–5123.
- [35] R. Alam, R. Bhowmick, A.S.M. Islam, A. Katarkar, K. Chaudhurib, M. Ali, A rhodamine based fluorescent trivalent sensor (Fe³⁺, Al³⁺, Cr³⁺) with potential applications for live cell imaging and combinational logic circuits and memory devices, *New J. Chem.* 41 (2017) 8359–8369.
- [36] P. Li, Y. Wang, A new fluorescent sensor containing glutamic acid for Fe³⁺ and its resulting complex as a secondary sensor for PPI in purely aqueous solution, *New J. Chem.* 41 (2017) 4234–4240.
- [37] C.-J. Hua, H. Zheng, K. Zhang, M. Xin, J.-R. Gao, Y.-J. Li, A novel turn off fluorescent sensor for Fe(III) and pH environment based on coumarin derivatives: the fluorescence characteristics and theoretical study, *Tetrahedron* 72 (2016) 8365–8372.
- [38] L.-Q. Li, Z.-H. Liu, A Colorimetric and Fluorescent Sensor for Iron Recognition Based on Rhodamine Derivative, *J. Fluoresc.* 27 (2017) 427–431.

- [39] S. Hua, S. Zhang, C. Gao, C. Xu, Q. Gao, A new selective fluorescent sensor for Fe³⁺ based on a pyrazoline derivative, *Spectrochim. Acta A* 113 (2013) 325–331.
- [40] M. Zhang, Y. Gao, M. Li, M. Yu, M. Li, L. Li, M. Zhu, J. Zhang, T. Yia, C. Huanga, A selective turn-on fluorescent sensor for Fe(III) and application to bioimaging, *Tetrahedron Lett.* 48 (2007) 3709–3712.
- [41] Q.-H. Luo, L.-J. Jiang, C.-Y. Duan, M.-C. Shen, H.-W. Hu, Y.-J. Liu, A new dioxotetraamine ligand appended with fluorenyl and its copper(II) complex. Synthesis, crystal structure and solution behavior, *Inorg. Chim. Acta* 295 (1999) 48–55.
- [42] M.J. Frisch, G.W. Trucks, H.B. Schlegel, G.E. Scuseria, M.A. Robb, J.R. Cheeseman, G. Scalmani, V. Barone, B. Mennucci, G.A. Petersson, H. Nakatsuji, M. Caricato, X. Li, H.P. Hratchian, A.F. Izmaylov, J. Bloino, G. Zheng, J.L. Sonnenberg, M. Hada, *GAUSSIAN* (2009).
- [43] Marcus D Hanwell, Donald E Curtis, David C Lonie, Tim Vandermeersch, Eva Zurek, Geoffrey R Hutchison, An advanced semantic chemical editor, visualization, and analysis platform, *J. Cheminformatics* 4 (1) (2012), <https://doi.org/10.1186/1758-2946-4-17>.
- [44] N.M. O'boyle, A.L. Tenderholt, K.M. Langner, cclib: a library for package-independent computational chemistry algorithm, *J. Comput. Chem.* 29 (2008) 839–845.
- [45] S.L.R. Ellison, V.J. Barwick, T.J.D. Farrant, *Practical Statistics for the Analytical Scientist - A Bench Guide*, 2nd ed., Royal Society of Chemistry, Cambridge, 2009.
- [46] J.N. Miller, J.C. Miller, *Statistics and Chemometrics for Analytical Chemistry* 5th ed., 2005. Edinburgh, Pearson - Prentice Hall Ptr.
- [47] D.B. Hibbert, J.J. Gooding, *Data analysis for chemistry - an introductory guide for students and laboratory scientists*, Oxford University Press: Printed in the United States of America, 2006.
- [48] D.N. Rutledge, A.S. Barros, Durbin-Watson statistic as a morphological estimator of information content, *Anal. Chim. Acta* 454 (2) (2002) 277–295.
- [49] H.A. Benesi, J.A. Hildebrand, A Spectrophotometric Investigation of the Interaction of Iodine with Aromatic Hydrocarbons, *J. Am. Chem. Soc.* 71 (1949) 2703–2704.
- [50] D.M. Roundhill (Ed.), *Photochemistry and Photophysics of Metal Complexes*, Springer US, Boston, MA, 1994.
- [51] B. Valeur, *Molecular Fluorescence: Principles and Applications*, Wiley-VCH, Weinheim, 2001.
- [52] J.R. Lakowicz, *Principles of Fluorescence Spectroscopy*, 2nd ed., Cambridge University Press, Cambridge, 1999.
- [53] A. Shylaja, S.S. Roja, R.V. Priya, R.R. Kumar, Four-component Domino Synthesis of Pyrazolo[3,4-*h*]quinoline-3-carbonitriles: "Turn-Off" Fluorescent Chemosensor for Fe³⁺ Ions, *J. Org. Chem.* 83 (2018) 14084–14090.
- [54] R. Azadbakht, N. Chehri, A new fluorescent macrocyclic nano-chemosensor for Fe³⁺ and Γ in aqueous solution, *New J. Chem.* 42 (2018) 17690–17699.
- [55] F.N. Moghadam, M. Amirasr, K. Eskandari, S. Meghdadi, A new disulfide Schiff base as versatile "OFF-ON-OFF" fluorescent-colorimetric chemosensor for sequential detection of CN⁻ and Fe³⁺ ions: Combined experimental and theoretical studies, *New J. Chem.* 43 (2019) 13536–13544.
- [56] S. Manigandan, A. Muthusamy, R. Nandhakumar, C.I. David, Recognition of Fe³⁺ by a new azine-based fluorescent "turn-off" chemosensor and its binding mode analysis using DFT, *J. Mol. Struct.* 1208 (2020), 127834.
- [57] V. Dangi, M. Baral, B.K. Kanungo, Photophysical Studies of a Catechol Based Polyfunctional Dipodal Chelator: Application of Optical Probe for Selective Detection of Fe(III), *J. Fluoresc.* 30 (2020) 1131–1149.
- [58] Anvisa (Agência Nacional de Vigilância Sanitária). *Guia para tratamento estatístico da validação analítica*, 2018.